Biosensors and Bioelectronics 97 (2017) 253–259

Contents lists available at ScienceDirect

Biosensors and Bioelectronics

journal homepage: www.elsevier.com/locate/bios

An ultrasensitive photoelectrochemical immunosensor for insulin detection based on BiOBr/Ag_2S composite by in-situ growth method with high visible-light activity

Dawei Fan*, Haoyuan Wang, Malik Saddam Khan, Chunzhu Bao, Huan Wang, Dan Wu, Qin Wei, Bin Du*

Key Laboratory of Interfacial Reaction & Sensing Analysis in Universities of Shandong, School of Chemistry and Chemical Engineering, University of Jinan, Jinan 250022, PR China

ARTICLE INFO

Keywords:
BiOBr
Ag_2S
In-situ growth
Insulin
Photoelectrochemical immunosensor

ABSTRACT

A novel ultrasensitive label-free immunosensor based on BiOBr/Ag_2S composite with high visible-light photoelectrochemical activity was prepared for the detection of insulin. After BiOBr was modified by thioglycolic acid, Ag_2S nanoparticles were grown in-situ on the surface of BiOBr hierarchical microspheres to first form novel BiOBr/Ag_2S composite. When ascorbic acid (AA) was used as an efficient electron donor for scavenging photo-generated holes, BiOBr/Ag_2S composite material showed excellent photoelectrochemical activity. In order to immobilize insulin antibody, adhesive polydopamine (PDA) film formed by self-polymerization of dopamine was fabricated onto BiOBr/Ag_2S modified electrode. Moreover, PDA film could further enhance the visible light absorption of BiOBr/Ag_2S. When the solutions of 0.08 mol $L^{-1}$$AgNO_3$ and 0.1 mol L^{-1} AA were selected respectively during fabrication and detection process of this sensor, the best photocurrent singles were obtained. Under the optimum experimental condition, the specific binding between insulin and antibody resulted in a decrease in photocurrent intensity and the intensity decreased linearly with the logarithm of insulin concentration in the range of 0.001–20 ng mL^{-1} with a detection limit of 0.2 pg mL^{-1}. The photoelectrochemical sensor ITO/BiOBr/Ag_2S/PDA/anti-Insulin/BSA/Insulin revealed facile preparation, high sensitivity, and acceptable reproducibility, which may have practical applications in the biosensor, clinical diagnosis of cancers, photocatalysis, and other related fields.

1. Introduction

Photoelectrochemical (PEC) immunoassay is a promising analytical technique and playing increasingly important roles in the detection of diverse biological targets due to its distinct advantages, such as rapid test, desirable sensitivity, low cost, simple devices and so forth (Brown et al., 1992; Wang et al., 2009a, 2009b; Freeman et al., 2013; Li et al., 2016). Efficient differentiation between excitation light source and detection signals contributes to low background interference and high sensitivity of the PEC analysis (Tu et al., 2011; Fan et al., 2015). In order to obtain rich photoelectrochemical materials with efficient PEC activity to fabricate immunosensors, many methods were employed *via* doping semiconductor with metallic or nonmetallic elements (Fan et al., 2015, 2016), sensitization with quantum dots (Fan et al., 2014a; Yang et al., 2015; Yue et al., 2013), and forming semiconductor heterojunctions (Chen et al., 2016). In the meanwhile, a series of ingenious sensing strategies have been developed for ultrasensitive detection of biomarkers, such as enhanced (Wen and Ju, 2016), quenched (Zhang et al., 2016) or blocked (Fan et al., 2014b, 2017) PEC phenomena through the interaction between substrate materials modified on the electrode and marked conjugates on the secondary antibodies (or modified strands of DNA).

TiO_2, and ZnO, as traditional semiconductor materials, have been applied widely in photoelectrochemical sensors, photocatalysis, photodegradation, and so on. However, the wide band-gaps of TiO_2 (3.2 eV) and ZnO (3.4 eV) make them show the weak visible-light response (Li et al., 2011; Das et al., 2013), and limit their applications. Bismuth oxybromide (BiOBr) has gained more attention of many researchers because of its hierarchical structures, physicochemical stability and new visible-light photocatalyst (Cheng et al., 2011; Xia et al., 2011; Wang et al., 2008). Although the band-gap of BiOBr is narrower (around 2.85 eV) than TiO_2 or ZnO. More efforts have been made in preparation of composites based on BiOBr in order to broaden its application, such as CdS/BiOBr (Cui et al., 2014), Ag/Ti-dope BiOBr (Jiang et al., 2012), and BiOBr-BiOI (Huang et al., 2015) composites.

* Corresponding authors.
E-mail addresses: jndxfandawei@126.com (D. Fan), dubin61@gmail.com (B. Du).

http://dx.doi.org/10.1016/j.bios.2017.05.044
Received 14 March 2017; Received in revised form 19 May 2017; Accepted 24 May 2017

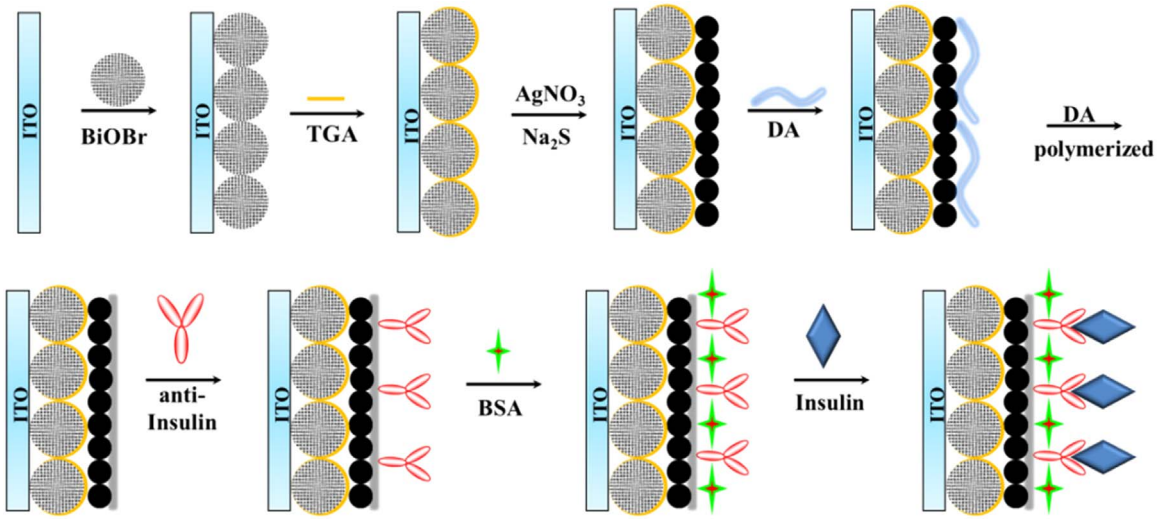

Fig. 1. Schematic representation of the preparation process of the PEC immunosensor.

Ag_2S nanomaterial, as a kind of low-toxic and narrow band-gap (about 1.0 eV) semiconductor (Neves et al., 2009), has been utilized increasingly in photocatalysis (Yadav and Jeevanandam, 2015), sensors (Zhang et al., 2014), and cell research (Hocaoglu et al., 2012). Moreover, the lower solubility product constant of Ag_2S makes it easy prepared and very stable, which contributes to fabrication of facile and stable sensors. Herein, we selected hierarchical BiOBr microflowers with high carrying capacity as the basic materials and then first prepared novel BiOBr/Ag_2S composite by in-situ growth method. The new BiOBr/Ag_2S modified ITO electrode shows excellent photoelectrochemical signal, which could lay the foundation for the fabrication of the sensitive PEC sensor.

Over here, a label-free photoelectrochemical immunosensor based on BiOBr/Ag_2S composite was fabricated, and expected to reach the goal of efficient determination of insulin. Insulin is an important polypeptide hormone, which is secreted by pancreatic β-cells, and plays an important role in maintaining blood glucose level in human beings (Habibi et al., 2016). In human, if insulin appears dysfunction, it will lead to diabetes mellitus. At the meantime, human also would be threatened with other kinds of diseases (Gobi et al., 2007). Consequently, the timely and accurate detection of insulin levels in serum is very important in monitoring and evaluation of the human condition, early warning of related diseases and another medical field (Yu et al., 2016). At present, the mainly detection methods of insulin level in serum include electrochemical immunoassay (Gerasimov et al., 2013), chromatography (Mercolini et al., 2008), radioimmunoassay (Murayama et al., 2006). In our work, this label-free PEC immunosensor system was developed and showed high sensitivity, good selectivity and stability, which exhibited its potential applications in many biological targets detection.

2. Experimental

2.1. Materials

Insulin and insulin antibody (anti-Insulin) were purchased from Shanghai Linc-Bio Science Co., Ltd. China. The details are shown in Electronic Supplementary Information (ESI†).

2.2. Apparatus

A 100 W LED lamp (white light) was employed as an irradiation source in the PEC test and its wavelength range was showed in Fig. S1 (ESI†). Scanning electron microscope (SEM) images and energy dispersive spectrometry (EDS) were obtained using a field emission SEM (Zeiss, Germany). X-ray diffraction (XRD) patterns were performed with D8 advance X-ray diffractometer (Bruker AXS, Germany). UV–vis diffuses reflectance spectra measurements were investigated with a Shimadzu UV-3101PC spectrometer (Japan). All PEC experiments were measured on a CHI760E electrochemical workstation (Chenhua Instrument Shanghai Co., Ltd, China). A three-electrode system was used, with a platinum wire as a counter-electrode, saturated calomel electrode as a reference electrode and modified ITO electrode (2.5 × 0.8 cm^2) as a working electrode. Electrochemical impedance spectroscopy (EIS) analysis was performed with an RST5200F electrochemical workstation (Zhengzhou Shiruisi Technology Co., Ltd, China) with a three-electrode system in a 5.0 mmol L^{-1} $[Fe(CN)_6]^{3-/4-}$ solution containing 0.10 mol L^{-1} KCl.

2.3. Synthesis of BiOBr

Bismuth oxybromide (BiOBr) were prepared by the reported solvothermal method (Cui et al., 2014). In detail, 1.9*g* $Bi(NO_3)_3 \cdot 5H_2O$ was dissolved in 70 mL ethylene glycol, and 2.9*g* hexadecyl trimethyl ammonium bromide (CTAB) was added to get a uniform suspension by stirring for one hour. Then, the suspension was transferred to the Teflon-lined autoclave and maintained at 140 °C for 8 h. The prepared precipitates were collected and washed by centrifugation with absolute ethanol and ultrapure water for more than 3 times and then dried at 80 °C for 8 h. In the end, the dried powder was calcined at 400 °C for 4 h and ground into powder for following use.

2.4. Fabrication of the label-free photoelectrochemical sensor

First of all, the ITO electrodes (2.5 × 0.8 cm^2) were successively washed for 30 min at 50 °C in series of ultrasonically solvents (acetone, ultrapure water, ethanol, and ultrapure water). The preparation process of the ultrasensitive PEC sensor is illustrated in Fig. 1. As follows, 10 μL of 4 mg mL^{-1} BiOBr aqueous suspension that was sonicated for 1 h was dropped onto a piece of ITO electrode. The modified electrode by BiOBr was dried naturally, followed by calcination at 400 °C for 1 h in a muffle oven. After then, 3 μL of 0.1 mol L^{-1} thioglycolic acid (TGA) aqueous solution was dropped on the BiOBr modified ITO electrode and dried under an infrared lamp for about 10 min. After rinsed with ultrapure water, the ITO/BiOBr/TGA electrode has been prepared successfully. 0.08 mol L^{-1} $AgNO_3$ solution 3 μL was dropped on the ITO/BiOBr/TGA electrode for 30 min in dark place, followed by thoroughly rinsing with ultrapure water to remove uncombined $AgNO_3$. Then, 3 μL of 0.1 mol L^{-1} Na_2S was dropped on the modified ITO electrode for 30 min to form Ag_2S sufficiently. After

rinsing with ultrapure water, the ITO/BiOBr/TGA/Ag_2S electrode was fabricated. Then, 4 μL 1 mg mL^{-1} dopamine (DA) in Tris-HCl solution (pH = 8.5) was dropped on the electrode for 1 h to form the polydopamine (PDA) film by self-polymerization of dopamine (Wan et al., 2011), followed by rinsing to remove the unreacted dopamine molecules. Dopamine has a unique molecular structure similar to the adhesive proteins of mussels: catechol and amine functional groups (Xu et al., 2010). In an alkalescent aqueous solution (pH 8.5), DA can easily self-polymerize to form polydopamine. Because the adhesion of the polydopamine is very strong, many biological molecules can connect immediately to the surface of PDA (Ma et al., 2015). Therefore, 4 μL of 1 μg mL^{-1} anti-Insulin solution was dropped onto the surface of ITO/BiOBr/TGA/Ag_2S/PDA electrode for 30 min under the room temperature. After washing the physically absorbed anti-Insulin, 4 μL of 1%BSA was dropped on the modified electrode for 30 min to block the nonspecific binding sites under the room temperature. Finally, when the electrode was washed completely, 4 μL of different concentrations of insulin in pH 7.4 PBS buffer solution was coated on the electrode for 30 min, followed by washing with water completely. So far, the ITO/BiOBr/Ag_2S/PDA/anti-Insulin/BSA/Insulin label-free PEC immunosensor has been constructed.

3. Results and discussion

3.1. Characterization of the BiOBr, BiOBr/Ag_2S

The morphologies of BiOBr and BiOBr/Ag_2S were characterized by scanning electron microscope (SEM). Fig. 2A shows that BiOBr has the hierarchical microsphere morphology, which were synthesized successfully according to the reference (Cui et al., 2014). SEM image of a large amount of BiOBr microspheres is showed in Fig. S2 (ESI†). The magnified images further display that the BiOBr hierarchical microspheres were composed of many nanosheets and nanoparticles (Fig. 2B). The hierarchical structure and uneven surface of BiOBr microspheres offered the large specific surface area and contributed to the in-situ growth of Ag_2S. Moreover, in order to have the strong binding between BiOBr and Ag_2S, TGA was coated on the surface of BiOBr. Fig. 2C reveals the surface structure of BiOBr does not change after modifying by TGA. Meanwhile, Fig. 2E shows the energy dispersive spectrometry (EDS) image of BiOBr/TGA/Ag_2S composite. The peaks of carbon and oxygen proved TGA had been bound on the surface of BiOBr due to the interaction between Bi atom in BiOBr and sulfhydryl group of TGA. As shown in Fig. 2D, Ag_2S nanoparticles were grown in-situ on the surface of TGA modified BiOBr hierarchical microspheres, which was covered by Ag_2S nanoparticles completely. The image of EDS image (Fig. 2E) also proved the successful synthesis of the BiOBr/Ag_2S composite.

Fig. 2F shows the UV–vis diffuse reflectance spectra of BiOBr, TGA, BiOBr/TGA, and BiOBr/TGA/Ag_2S composite. The absorption wavelength of BiOBr is under 420 nm wavelength, which reveals the weak and narrow absorption of BiOBr towards the visible-light. TGA aqueous solution is colorless. The absorption wavelength of TGA is below 400 nm, which mainly absorbs the ultraviolet light. However, when testing the sample of TGA modified BiOBr, a strong absorption in the visible light region is observed. Comparing with BiOBr and TGA, the absorption spectrum of BiOBr/TGA occurs to redshift obviously. In addition, the BiOBr/TGA composite is yellow, which should be ascribed to the interaction between the Bi atoms of BiOBr and the sulfhydryl group of TGA. After Ag_2S deposited on BiOBr/TGA material, the obtained BiOBr/TGA/Ag_2S composite shows wider and stronger absorption to visible light.

The crystalline nature of BiOBr and BiOBr/Ag_2S were studied using X-ray diffraction (XRD) analysis (Fig. 3). The diffraction spectrum of BiOBr shows the main peak of BiOBr could match with the standard PDF cards (PDF# 51-1161) completely and also agree with the peak of BiOBr in the reference report at 25.2°, 31.7°, 32.2°, 46.2°, 57.1° and

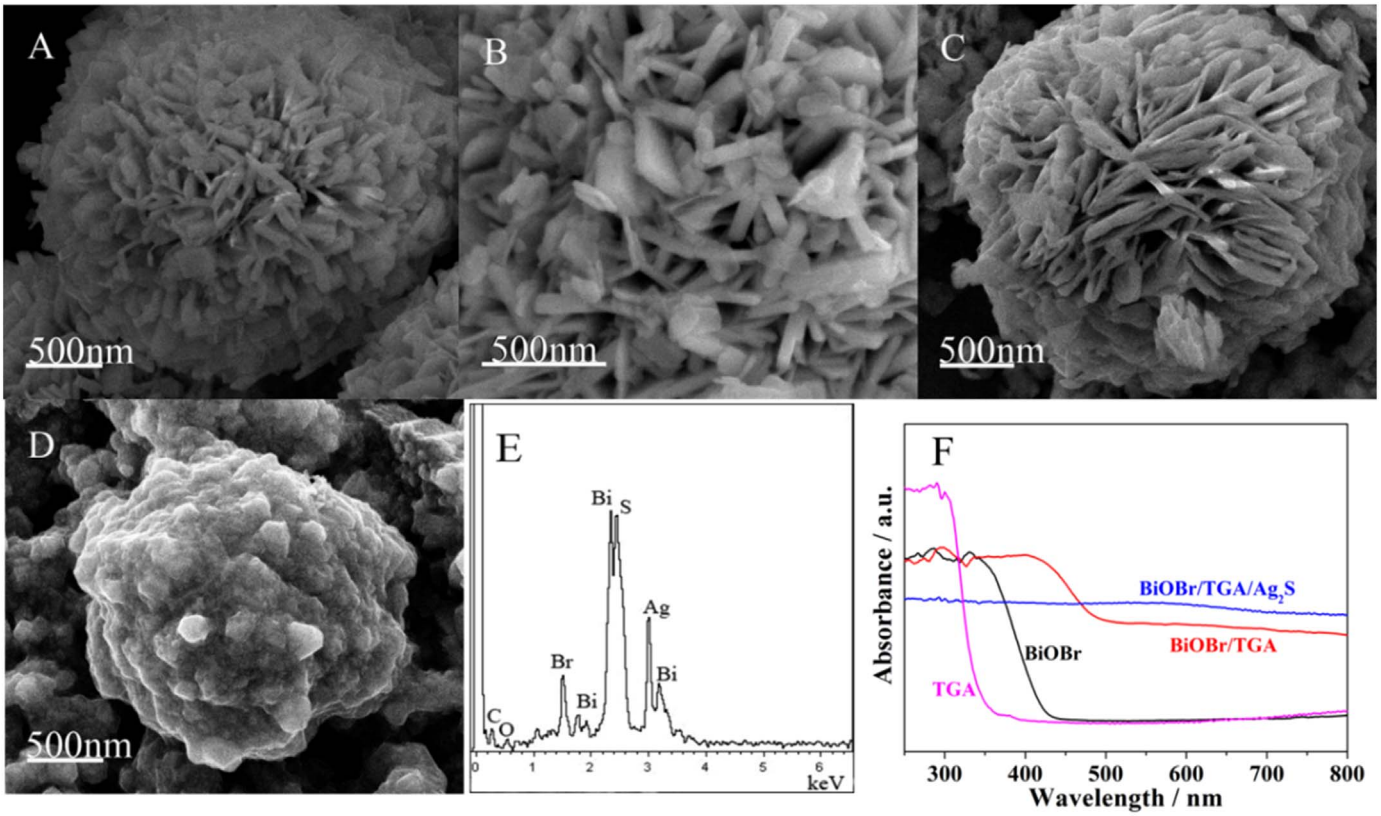

Fig. 2. SEM images of BiOBr (A, B), BiOBr/TGA (C), BiOBr/TGA/Ag_2S(D). EDS image of BiOBr/TGA/Ag_2S (E). UV–vis diffuse reflectance spectra of BiOBr, TGA, BiOBr/TGA, BiOBr/TGA/Ag_2S (F).

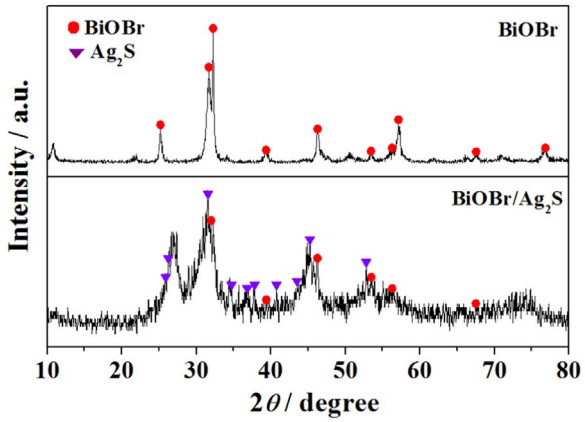

Fig. 3. XRD pattern of BiOBr and BiOBr/Ag_2S.

others (Cui et al., 2014). It confirms that the microflower-type BiOBr particles have been synthesized successfully. When comparing the diffraction spectra of BiOBr/Ag_2S with BiOBr, the signal peaks of BiOBr could be found obviously. At the meanwhile, referring the standard PDF card of Ag_2S (PDF# 14-0072), the peaks of Ag_2S also could be observed in the diffraction spectra of BiOBr/Ag_2S at 25.90°, 26.34°, 31.54°, 34.7°, 36.86°, 37.76°, 40.78°, 43.5°, 45.2°, 52.8° (Yadav and Jeevanandam, 2015). It also proved that Ag_2S nanoparticles were assembled on the BiOBr microspheres successfully. The poor crystalline nature of Ag_2S is proved from diffraction spectrum of BiOBr/Ag_2S, which is attributed to obtained nanoparticles of Ag_2S by in-situ growth method in accordance with SEM images.

3.2. Characterization of the immunosensor

The modified electrodes were tested by the photocurrent response and electrochemical impedance spectroscopy (EIS) to study the state of connection between composite material and ITO electrode, further exploring the condition of building the immunosensor. In addition, in order to obtain high and stable photocurrent signal, a certain amount of ascorbic acid (AA) was added to the testing environment. AA is a widely used excellent antioxidants with the oxidation potential of −0.185 V (vs. SCE) (Dawson et al., 1986). As the electron donation, AA can be oxidized by the holes generated by illuminated Ag_2S nanoparticles, which facilitates the separation of photo-generated holes and electrons (h^+/e^-) to get perfect photocurrent response (Wang et al., 2009a).

Under the visible-light excitation, the photoelectric behavior of the modified electrodes was investigated. Fig. 4A and B show the photocurrent-time curve of the modified electrode designed as a sensor to detect insulin. The photocurrent signal of bare ITO electrode (a) is the weakest, almost as zero. Compared with the bare ITO, the photocurrent signal of ITO/BiOBr is little higher. After modified by TGA, the photocurrent signal of ITO/BiOBr/TGA electrode is further enhanced than that of the pure BiOBr. The phenomenon also proves TGA has been modified on the surface of BiOBr. To our surprised, the photocurrent signal of ITO/BiOBr/TGA/Ag_2S electrode is excellent to reach 107 μA (d). It shows that Ag_2S nanoparticles are grown firmly on the surface of BiOBr to form the BiOBr/Ag_2S composite with perfect photoelectrochemical activity by in-situ growth method. Moreover, Ag_2S as a narrow bandwidth of semiconductor material improves the photoelectric response of BiOBr distinctly. Then, after modifying PDA on the composite materials, the photocurrent signal reaches 129 μA (e). The phenomenon could be ascribed to that phenolic hydroxyl groups on the surface of PDA have reducibility, which is helpful to reduce photo-generated holes to fulfill the separation photo-generated holes/electrons. When anti-insulin (f), BSA (g), and insulin (h) are modified onto the surface of the ITO electrode successively, the photocurrents reduce gradually. Protein molecules such as anti-insulin, BSA and insulin are insulating, which prevent AA from combining with photo-generated holes of Ag_2S, and cause the recombination of photo-generated holes/electrons more easily and result in a reduction of the photocurrent. As a result, when the insulin was connected with anti-insulin by the specific recognition between antigen and antibody, the photocurrent intensity reduced obviously to 54 μA (h), comparing with the photocurrent 96 μA (g) of ITO/BiOBr/TGA/Ag_2S/PDA/anti-Insulin/BSA electrode. These phenomena demonstrate the successful fabrication of the photoelectrochemical immunosensor based on BiOBr/Ag_2S composite for the detection of insulin.

To deeply analyze the construction process of label-free photoelectrochemical sensor, the EIS analysis was carried out in the solution of 5.0 mmol L^{-1} $[Fe(CN)_6]^{3-/4-}$ including 0.1 mol L^{-1} KCl. The EIS Nyquist plots of layer-by-layer modified ITO electrodes are shown in Fig. 4C. And the inset in Fig. 4C is Randles equivalent circuit, which contains the electrode transfer resistance (R_{et}), the resistance of solution (R_s), the double layer capacitance (C_{dl}), and the Warburg impedance (Z_ω). The values of them were fitted with ZSimWin software. The EIS can effectively describe R_{et}, with the constant modification of electrode, the value of the resistance also change (An et al., 2010; Gao et al., 2011). Typically, EIS diagram consists of two parts: one part is the restrictions in the process of high frequency semicircle part; the other part is the linear part of low frequency in the process of diffusion. The diameter of the semicircle in the high frequency part can directly response R_{et} value (Gao et al., 2015). The R_{et} value of bare ITO electrode was small because of its certain conductivity (a). When modifying BiOBr on the ITO, R_{et} value increased significantly (b), implying its successful fabrication of ITO/BiOBr electrode. After combining TGA to BiOBr surface, dissociated H^+ form TGA maybe accelerate the electron transfer of the electronic mediator ($[Fe(CN)_6]^{3-4-}$, and improve the conductivity. So, R_{et} value reduced significantly. Ag_2S modified on BiOBr/TGA is a kind of semiconductor material and blocks electron transfer, then R_{et} value of BiOBr/TGA/Ag_2S increases (d). Because the PDA is polymers, which also could hinder the electrons from transferring to the electrode, R_{et} value further augments slightly after modifying PDA on the previous electrode (e). The modifications of protein macromolecules with good insulation on the electrode surface improve the R_{et} values obviously, such as anti-Insulin (f), BSA (g), and Insulin (h). The phenomena also proved that the assembly process of photoelectrochemical immunosensor was very successful.

On the basis of the above results, the energy levels of Ag_2S nanoparticles prepared by in-situ growth and BiOBr hierarchical microspheres could match perfectly with each other, which results in the high photocurrent signal of BiOBr/Ag_2S composite. Under irradiation of visible-light, electron transfer mechanism of PEC sensor based on BiOBr/Ag_2S in PBS electrolyte containing AA is shown in Fig. 4D. According to the reference (Cui et al., 2014), the band-gap of BiOBr material is 2.85 eV, and the separation of photo-generated holes/electrons is inefficient under the visible light. Ag_2S nanoparticles as a narrow band-gap of 1.0 eV semiconductor, the electrons transition can occur easily under the visible light. When the novel composite is prepared by in-situ growth of Ag_2S nanoparticles on BiOBr hierarchical microspheres, a visible-light active Ag_2S/BiOBr composite was fabricated. The UV–vis diffuse reflectance spectra also confirm the better absorption of Ag_2S/BiOBr composite than that of pure BiOBr to the visible light. Moreover, AA as an inhibitor clears photo-generated holes to stabilize and promote the photocurrent signals. Based on this, a sensitive, high-performance photoelectrochemical sensor is constructed successfully.

3.3. Optimization of the experimental conditions

For more sensitive detection of insulin by the constructed sensor in the actual test, the test conditions are optimized, including the concentration of AA and $AgNO_3$ solution. From Fig. S3A (ESI†), the

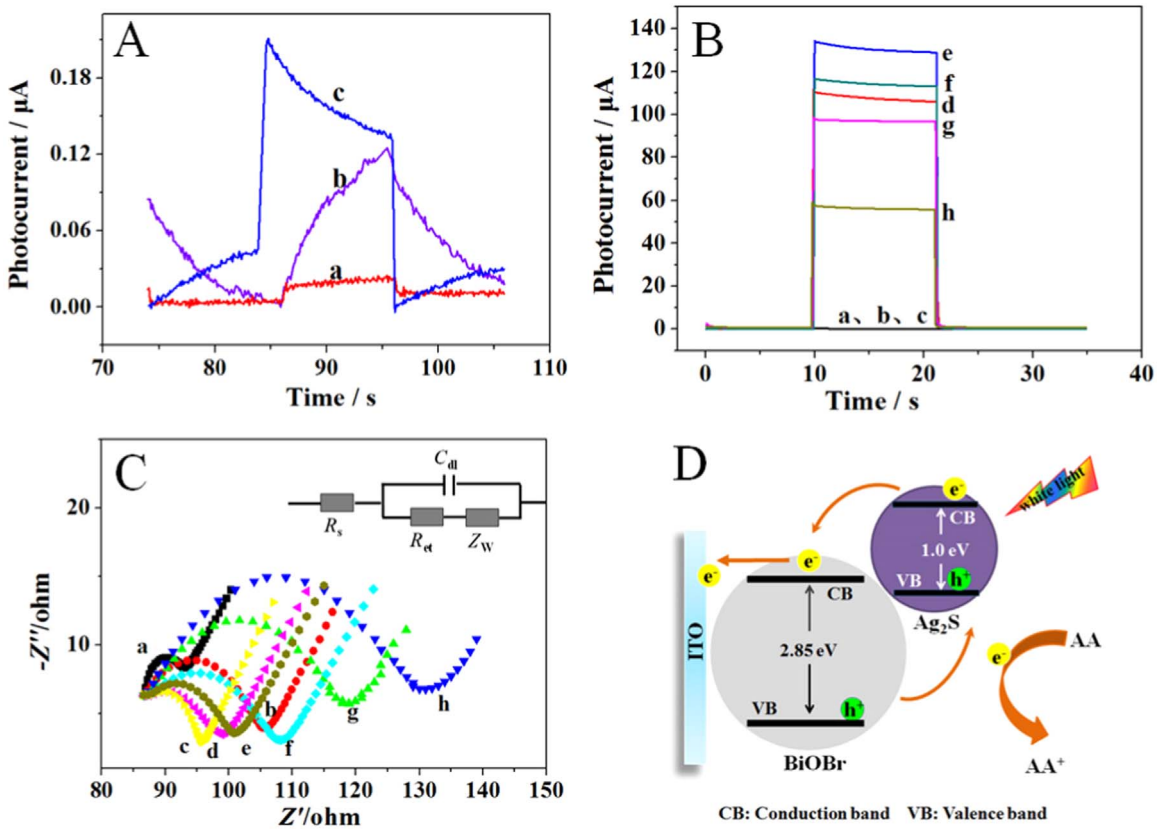

Fig. 4. (A) (B) the photocurrent response, (C) EIS image of the electrode by layer-by-layer assembly. (a) ITO, (b) ITO/BiOBr, (c) ITO/BiOBr/TGA, (d) ITO/BiOBr/TGA/Ag_2S, (e) ITO/BiOBr/TGA/Ag_2S/PDA, (f) ITO/BiOBr/TGA/Ag_2S/PDA/anti-Insulin, (g) ITO/BiOBr/TGA/Ag_2S/PDA/anti-Insulin/BSA, (h) ITO/BiOBr/TGA/Ag_2S/PDA/anti-Insulin/BSA/Insulin. (D) Electron-transfer mechanism of PEC sensor based on BiOBr/Ag_2S composite in PBS electrolyte containing AA.

concentration of the $AgNO_3$ aqueous solution is optimized ranging from 0.01 to 0.1 mol L^{-1}. The photocurrent arrives at the maximum value when the concentration of the $AgNO_3$ solution is 0.08 mol L^{-1} but reduces at the concentration of $AgNO_3$ higher than 0.08 mol L^{-1}. In this experiment, Ag_2S precipitation was occurred in-situ on the surface of BiOBr microspheres, by reacting $AgNO_3$ and Na_2S solution. When the concentration of $AgNO_3$ is 0.08 mol L^{-1}, the amount of Ag_2S formed on the surface of BiOBr/TGA reaches saturation. But more Ag_2S nanoparticles could hinder the electrons transfer because of lower conductivity caused by thicker materials. In the meantime, excessive Ag_2S nanoparticles as a narrow band-gap lead to the high ratio of recombination of photo-generated holes/electrons. Therefore, the photocurrent signal of the composite material decreases obviously. Therefore, 0.08 mol L^{-1} $AgNO_3$ was used in the subsequent experiment. From Fig. S3B (ESI†), it is clear that the photocurrent signal of ITO/BiOBr/TGA/Ag_2S/PDA is very low without AA in an electrolyte. But when the concentration of AA increases to 0.1 mol L^{-1}, photocurrent signal becomes a higher value of 129 μA. It shows that AA as a perfect electron donor prevented recombination of the photo-generated holes/electrons to promote photo-generated carrier transmission. With the increase of the AA concentration, photocurrent signal was also rising, when the concentration of AA was 0.1 mol L^{-1}, the photocurrent signal arrives at the optimum value. So, 0.1 mol L^{-1} AA and 0.08 mol $L^{-1}$$AgNO_3$ solutions were selected as optimum experimental conditions.

3.4. Photoelectrochemical behavior of target insulin detection

The PEC immunosensor was applied for the determination of insulin with various concentrations with the optimum testing conditions. From Fig. 5A, it is clear that the photocurrents decline gradually with the increase of the insulin concentration, which owns to the increase of insulin combined to the ITO/BiOBr/TGA/Ag_2S/PDA/anti-Insulin/BSA electrode through specific recognition between insulin and insulin antibody. Moreover, as is displayed in Fig. 5B, the photocurrent signals reduced linearly with the logarithm of the concentration of insulin ranging from 0.001 ng mL^{-1} to 20 ng mL^{-1}. The linear equation is I = 59.73–10.54 log ($c_{insulin}$, ng mL^{-1}) with a linear correlation coefficient of 0.993. Meanwhile, the limit of detection (LOD, S/N=3) is 0.2 pg mL^{-1}. Table S1 (ESI†) shows a comparison with other methods for the detection of insulin. The PEC immunosensor we fabricated can reach much lower limit of detection and wider detection linear range than those of other methods such as electrochemical analysis, electrochemical impedance spectroscopy analysis and flow injection analysis. Also, we obtained comparable property with the other PEC immunosensor.

The stability test as shown in Fig. 5C. Under 15 times on/off LED light irradiation cycles, the photocurrent response does not vary obviously. It implies that this PEC immunosensor has good stability, which could be applied in repeatable and long-time tests. Moreover, under the same experimental conditions, five ITO electrodes were assembled into immunosenor to detect 0.1 ng mL^{-1} of insulin. The relative standard deviation (RSD) of five times test was 2.0% (68.50 μA, 69.81 μA, 68.93 μA, 70.72 μA, 71.92 μA). The results showed the PEC immunosensor has good reproducibility.

The selectivity of the novel PEC immunosensor for insulin determination was carried out to testify its practical values. Therefore, the photocurrent signals were researched by mixing 0.1 ng mL^{-1} of insulin with 10 ng mL^{-1} of prostate specific antigen (PSA), 10 ng mL^{-1} carcinoembryonic antigen (CEA), and 10 ng mL^{-1} squamous cell carcinoma antigen (SCCA). From Fig. 5D, it is clear that no obvious interferential photocurrent signal was obtained when 10 ng mL^{-1} of PSA, CEA and

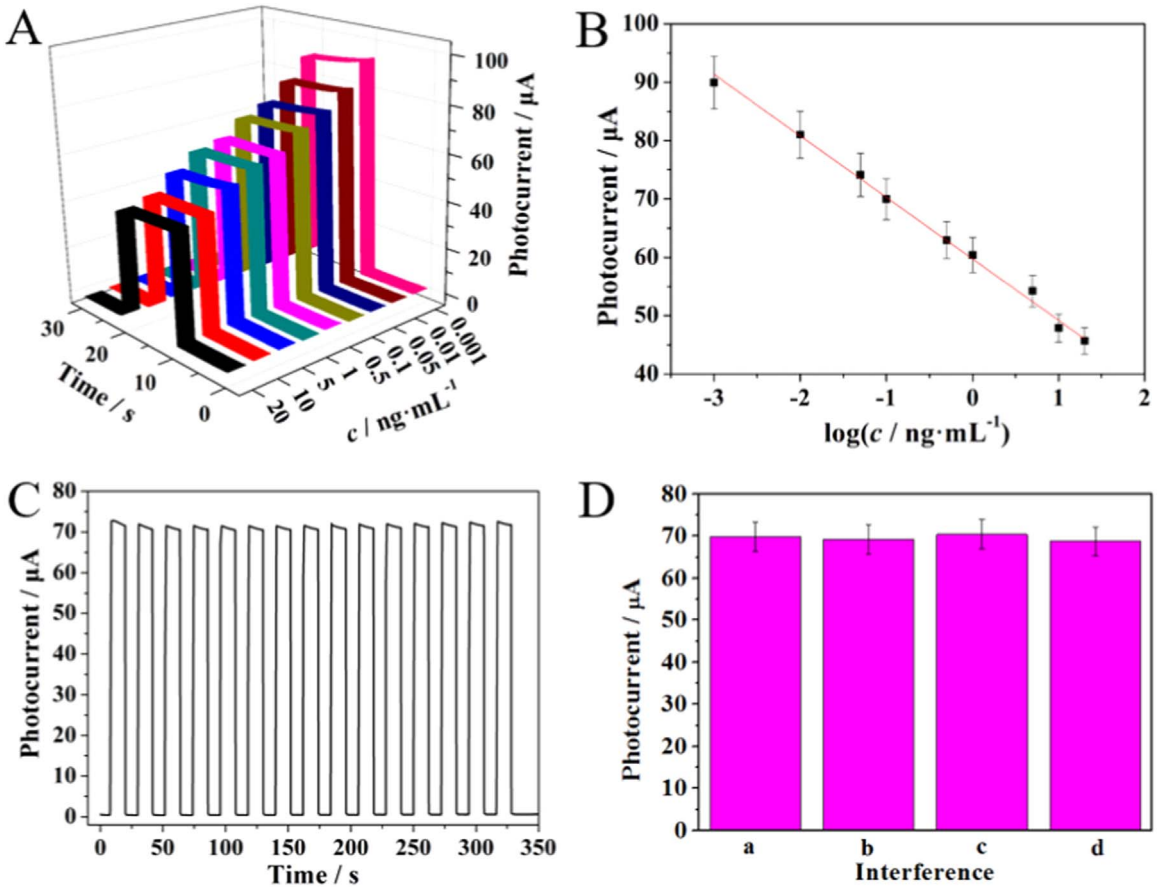

Fig. 5. Photocurrent response curves (A) and calibration curve (B) of PEC immunosensor for the determination of various concentrations of insulin. (C) Time based photocurrent response of the immunosensor repeated every 10 s under 15 times on/off irradiation cycles, $c_{insulin}$=0.1 ng mL^{-1}. (D) Selectivity of the developed PEC sensor to insulin. (a) 0.1 ng mL^{-1} insulin, (b) 0.1 ng mL^{-1} insulin +10 ng mL^{-1} PSA, (c) 0.1 ng mL^{-1} insulin +10 ng mL^{-1} CEA, (d) 0.1 ng mL^{-1} insulin +10 ng mL^{-1} SCCA. The applied potential was 0 V.

SCCA was incubated on the ITO/BiOBr/TGA/Ag_2S/PDA/anti-Insulin/BSA electrode mixed with 0.1 ng mL^{-1} SCCA, which showed good selectivity of the PEC immunosensor for insulin detection.

3.5. Application of the immunosensor in human serum

To evaluate the practical applications of the suggested PEC biosensor, the recoveries of different concentrations of insulin (0.5, 1.0 and 2.0 ng mL^{-1}) in human blood serum samples obtained from University of Jinan Hospital were studied by standard addition methods. Table 1 showed that the determined insulin concentration of the real sample was 0.26 ng mL^{-1}, the relative standard deviation (RSD) was in the range of 2.2–4.1%, and the average recoveries of the immunosensor samples were in the range of 97.2–100.7%. Table S2 (ESI†) shows a comparison of the RSD with other methods for the detection of insulin. The property of our PEC sensor is comparable to others. These acceptable results display that the suggested PEC sensor has potential practical value in blood sample determination.

Table 1
The results of the insulin detection in the human serum sample.

Content of insulin in serum samples (ng mL^{-1})	Added content (ng mL^{-1})	The detection content (ng mL^{-1})	RSD (%)	Recovery (%)
0.26	0.50	0.74, 0.71, 0.79, 0.76, 0.73	4.1	97.2
	1.00	1.26, 1.19, 1.24, 1.27, 1.29	3.0	99.0
	2.00	2.19, 2.27, 2.32, 2.29, 2.30	2.2	100.7

4. Conclusion

In summary, BiOBr/Ag_2S composite material with high visible-light activity was successfully synthesized by in-situ growth method. Polydopamine film modified on the electrode not only served as the linker of anti-insulin, but also enhanced the photoelectric response of BiOBr/Ag_2S composite. Then, an ultrasensitive label-free photoelectrochemical immunosensor based on the BiOBr/Ag_2S for detection of insulin was proposed. The immunosensor detected insulin in the range of 0.001 ng mL^{-1}–20 ng mL^{-1} with a low limit of detection (0.2 pg mL^{-1}), with having high reproducibility and perfect stability. The novel and convenient photoelectrochemical immunosensor displayed potential application in analytic detection, biosensor and PEC studies.

Acknowledgments

This research was supported by the National Key Scientific Instrument and Equipment Development Project of China (No. 21627809), National Natural Science Foundation of China (Nos. 21575050, 21375047, 21405059), the China Postdoctoral Science Foundation (2016M592122), the Postdoctoral Science Foundation of Shandong Province (201603060), the Postdoctoral Science Foundation of University of Jinan (XBH1517), the Science and Technology Plan Project of Jinan (No. 201307010), Qin Wei thanks the Special Foundation for Taishan Scholar Professorship of Shandong Province and UJN (No. ts20130937).

Appendix A. Supporting information

Supplementary data associated with this article can be found in the online version at doi:10.1016/j.bios.2017.05.044.

References

An, Y.R., Tang, L.L., Jiang, X.L., Chen, H., Yang, M.C., Jin, L.T., Zhang, S.P., Wang, C.G., Zhang, W., 2010. Chem. Eur. J. 16, 14439–14446.

Brown, G.N., Birks, J.W., Koval, C.A., 1992. Anal. Chem. 64, 427–434.

Chen, D.Y., Jiang, D., Du, X.J., Zhou, L., Huang, L.Y., Qian, J., Liu, Q., Hao, N., Li, Y.P., Wang, K., 2016. Electrochim. Acta 215, 305–312.

Cheng, H.F., Huang, B.B., Wang, P., Wang, Z.Y., Lou, Z.Z., Wang, J.P., Qin, X.Y., Zhang, X.Y., Dai, Y., 2011. Chem. Commun. 47, 7054–7056.

Cui, W., An, W., Liu, L., 2014. Appl. Surf. Sci. 319, 298–305.

Das, S.C., Green, R.J., Podder, J., Regier, T.Z., Chang, G.S., Moewes, A., 2013. J. Phys. Chem. C. 117, 12745–12753.

Dawson, R.M.C., Elliott, D.C., Elliott, W.H., Jones, K.M., 1986. Data for Biochemical Research 2nd ed. Oxford Science Publications, Clarendon Press, Oxford.

Fan, D.W., Guo, C.J., Ma, H.M., Zhao, D., Li, Y.N., Wu, D., Wei, Q., 2016. Biosens. Bioelectron. 75, 116–122.

Fan, D.W., Ren, X., Wang, H.Y., Wu, D., Zhao, D., Chen, Y.C., Wei, Q., Du, Bin, 2017. Biosens. Bioelectron. 87, 593–599.

Fan, D.W., Wu, D., Cui, J.L., Chen, Y.C., Ma, H.M., Liu, Y.X., Wei, Q., Du, B., 2015. Biosens. Bioelectron. 74, 843–848.

Fan, G.C., Han, L., Zhang, J.R., Zhu, J.J., 2014a. Anal. Chem. 86, 10877–10884.

Fan, G.C., Han, L., Zhu, H., Zhang, J.R., Zhu, J.J., 2014b. Anal. Chem. 86, 12398–12405.

Freeman, R., Girsh, J., Willner, I., 2013. ACS Appl. Mater. Interfaces 5, 2815–2834.

Gao, E.P., Wang, W.Z., Shang, M., Xu, J.H., 2011. Phys. Chem. Chem. Phys. 13, 2887–2893.

Gao, P.C., Ma, H.M., Yan, T., Wu, D., Ren, X., Yang, J.J., Du, B., Wei, Q., 2015. Dalton Trans. 44, 773–781.

Gerasimov, J.Y., Schaefer, C.S., Yang, W.W., Grout, R.L., Lai, R.Y., 2013. Biosens. Bioelectron. 42, 62–68.

Gobi, K.V., Iwasaka, H., Miura, N., 2007. Biosens. Bioelectron. 22, 1382–1389.

Habibi, E., Omidinia, E., Heidari, H., Fazli, M., 2016. Anal. Biochem. 495, 37–41.

Hocaoglu, I., Çizmeciyan, M.N., Erdem, R., Ozen, C., Kurt, A., Sennaroglu, A., Acar, H.Y., 2012. J. Mater. Chem. 22, 14674–14681.

Huang, H.W., Han, X., Li, X.W., Wang, S.C., Chu, P.K., Zhang, Y.H., 2015. ACS Appl. Mater. Interfaces 7, 482–492.

Jiang, G.H., Wang, R.J., Wang, X.H., Xi, X.G., Hu, R.B., Zhou, Y., Wang, S., Wang, T., Chen, W.X., 2012. ACS Appl. Mater. Interfaces 4, 4440–4444.

Li, H.B., Li, J., Xu, Q., Hu, X.Y., 2011. Anal. Chem. 83, 9681–9686.

Li, H.B., Qiao, Y.F., Li, J., Fang, H.L., Fan, D.H., Wang, W., 2016. Biosens. Bioelectron. 77, 378–384.

Ma, H.M., Yan, T., Zhang, Y., Gao, P.C., Pang, X.H., Du, B., Wei, Q., 2015. Analyst 140, 5019–5022.

Mercolini, L., Musenga, A., Saladini, B., Bigucci, F., Luppi, B., Zecchi, V., Raggi, M.A., 2008. J. Pharm. Biomed. 48, 1303–1309.

Murayama, H., Matsuura, N., Kawamura, T., Maruyama, T., 2006. J. Autoimmun. 26, 127–132.

Neves, M.C., Nogueira, J.M.F., Trindade, T., Mendonça, M.H., Pereira, M.I., Monteiro, O.C., 2009. J. Photoch. Photobio. A. 204, 168–173.

Tu, W.W., Lei, J.P., Wang, P., Ju, H.X., 2011. Chem. Eur. J. 17, 9440–9447.

Wan, Y., Zhang, D., Wang, Y., Qi, P., Hou, B.R., 2011. Biosens. Bioelectron. 26, 2595–2600.

Wang, G.L., Xu, J.J., Chen, H.Y., Fu, S.Z., 2009a. Biosens. Bioelectron. 25, 791–796.

Wang, G.L., Yu, P.P., Xu, J.J., Chen, H.Y., 2009b. J. Phys. Chem. C. 113, 11142–11148.

Wang, W.D., Huang, F.Q., Lin, X.P., Yang, J.H., 2008. Catal. Commun. 9, 8–12.

Wen, G.M., Ju, H.X., 2016. Anal. Chem. 88, 8339–8345.

Xia, J.X., Yin, S., Li, H.M., Xu, H., Xu, L., Xu, Y.G., 2011. Dalton Trans. 40, 5249–5258.

Xu, L.Q., Yang, W.J., Neoh, K.-G., Kang, E.-T., Fu, G.D., 2010. Macromolecules 43, 8336–8339.

Yadav, S.K., Jeevanandam, P., 2015. J. Alloy. Compd. 649, 483–490.

Yang, J.J., Gao, P.C., Liu, Y.X., Li, R.X., Ma, H.M., Du, B., Wei, Q., 2015. Biosens. Bioelectron. 64, 13–18.

Yu, Y.N., Guo, M., Yuan, M.W., Liu, W.T., Hu, J.B., 2016. Biosens. Bioelectron. 77, 215–219.

Yue, Z., Lisdat, F., Parak, W.J., Hickey, S.G., Tu, L.P., Sabir, N., Dorfs, D., Bigall, N.C., 2013. ACS Appl. Mater. Interfaces 5, 2800–2814.

Zhang, L., Sun, Y., Liang, Y.Y., He, J.P., Zhao, W.W., Xu, J.J., Chen, H.Y., 2016. Biosens. Bioelectron. 85, 930–934.

Zhang, X.R., Liu, M.S., Liu, H.X., Zhang, S.S., 2014. Biosens. Bioelectron. 56, 307–312.